Rashba spin splitting in parabolic quantum dots

Johnson Lee, Harold N. Spector, Wu Ching Chou, and Chon Saar Chu

Articles you may be interested in

Magneto-optics of single Rashba spintronic quantum dots subjected to a perpendicular magnetic field: Fundamentals
J. Appl. Phys. **104**, 083714 (2008); 10.1063/1.3003086

Electron and hole spin dynamics in semiconductor quantum dots
Appl. Phys. Lett. **86**, 113111 (2005); 10.1063/1.1857067

Energy levels of a parabolically confined quantum dot in the presence of spin-orbit interaction
J. Appl. Phys. **95**, 6368 (2004); 10.1063/1.1710726

Magnetic properties of parabolic quantum dots in the presence of the spin–orbit interaction
J. Appl. Phys. **94**, 5891 (2003); 10.1063/1.1614426

Absorption of surface acoustic waves by a two-dimensional electron gas in the presence of spin-orbit interaction
J. Appl. Phys. **94**, 3229 (2003); 10.1063/1.1599631

Rashba spin splitting in parabolic quantum dots

Johnson Lee[a)] and Harold N. Spector
Department of Physics, Illinois Institute of Technology, Chicago, Illinois 60616

Wu Ching Chou and Chon Saar Chu
Department of Electrophysics, National Chiao Tung University, Hsin-Chu, Taiwan 30010, Republic of China

We have investigated the effect of the Rashba spin splitting and a magnetic field on the energy levels of electrons in parabolic quantum dots. We find that with an increase in the Rashba parameter, the spin-orbit interaction mixes states of higher angular momentum together. In the absence of a magnetic field, the energy levels of the electrons are doubly degenerate and decrease as the Rashba parameter increases. In the presence of a magnetic field, this degeneracy is removed and the energy splitting of the spin states increases with the increase in both the Rashba parameter and the magnetic field. The Fermi energy level as a function of the magnetic field shows oscillatory behavior due to the crossings between the energy levels of the system. The magnetization of the electron gas is investigated and shows strong oscillations with the magnetic field for large values of the Rashba parameter. © *2006 American Institute of Physics*. [DOI: 10.1063/1.2201847]

I. INTRODUCTION

The exploration of spintronics (spin electronics) for quantum computing[1–3] is one of the most exciting fields for future developments in high-speed computing and data storage. The use of spin states rather than charge states as quantum bits in semiconductor materials is attractive because the spin state is insensitive to electronic noise in the device environment.[4] The polarization of the spins is expected to last long enough at low temperatures so that quantum computation can be carried out. It has been demonstrated that controlled spin transfers between electrons are possible in a spin-polarized two-dimensional electron gas (2DEG).[5] The Rashba[6] spin-orbit interaction (SOI) due to the lack of inversion symmetry caused by the confinement potential is considered as a possible mechanism to control and manipulate electron states via gate voltages.[7–11] It is also the basis of the spin dependent field-effect transistor (spinFET) proposed by Datta and Das.[12] In order to gain better insight of the influence of the electron spin on the carrier transport in nonmagnetic semiconductor nanostructures, considerable research has been done on the fundamental physics and application aspects of the problem. The effect of a magnetic field on the transport properties in low dimensional nanostructures (quantum wells, wires, and dots) with the Rashba SOI has been investigated both experimentally[9–11] and theoretically.[13–24] One of the major tasks of the theoretical investigations has been to evaluate the electron energy spectra for the nanostructures in the presence of the Rashba SOI by using the two-band[13–24] and eight-band[25] models. Recently, theoretical investigations of the SOI effects in a parabolic quantum dot were reported using the two-band model for the low field magnetization including the electron-electron interaction effects by Chakraborty and Pietläinen[22]

and for the energy levels by Kuan *et al.*[21] Debald and Emary[23] have shown, using a model that is formally equivalent to that of Jaynes and Cummings,[24] that the SOI can couple two states of adjacent angular momentum and opposite spin which results in a energy splitting.

The main purpose of this paper is to study the influence of the Rashba SOI on the energy levels of parabolic quantum dots in magnetic fields. To solve the one particle Schrödinger equation for electron spins (up and down), we adopt the wave functions proposed in Refs. 22 and 26 in polar coordinates. We show that the assumption that the angular momentum quantum number m is a good quantum number made in Ref. 21 is incorrect in the presence of the Rashba SOI. To ensure the correctness of the numerical results, we also solve the same problem in the x-y coordinate system. In order to study the variation of the Fermi energy level and the magnetization as functions of the magnetic field, 30 quantized energy levels of the system are used.

II. TWO-BAND MODEL

Consider an InAs/GaAs quantum disk in the x-y plane and a magnetic field B applied in the crystal growth z direction. A quantum disk is formed by assuming that all carriers are completely confined in the z direction and laterally confined by a parabolic confinement potential[27] $V_c(x,y)$. The spin dependence of the electron transport across the nonmagnetic semiconductor heterostructures arises due to the Rashba SOI. Because of the complete confinement of the carrier in the z direction, the wave vector is taken to be $\mathbf{k}=(k_x,k_y,k_z)$ with $k_z=0$. The single electron Hamiltonian for electron spins (up and down) in the two-band model is given by

---
[a)]Electronic mail: johnson.lee@iit.edu

$$H = \frac{1}{2m^*}(\mathbf{p} - e\mathbf{A})^2 + \frac{\alpha}{\hbar}[\boldsymbol{\sigma} \times (\mathbf{p} - e\mathbf{A})]_z + \frac{1}{2}g\mu_B\sigma_z B$$

$$+ V_c(x,y), \tag{1}$$

with $V_c(x,y) = m^*\omega_0^2(x^2+y^2)/2$, where $\mathbf{p} = \hbar\mathbf{k}$ is the electron momentum, m^* is the electron effective mass, α is the Rashba parameter for the spin-orbit interaction, $\boldsymbol{\sigma} = (\sigma_x, \sigma_y, \sigma_z)$ is the Pauli spin matrices, ω_0 is the characteristic angular frequency of the confinement potential,[27] $\mathbf{A} = \frac{1}{2}\mathbf{B}(-y,x,0)$ is the vector potential in one of the Landau gauges, μ_B is the Bohr magneton, and g is the Landé factor of the electron. The choice of $\mathbf{A}$ guarantees that $\mathbf{B} = \mathrm{curl}\mathbf{A}$ holds. For convenience in the numerical calculations, we choose the effective atomic units $\mathrm{Ry}^* = \mathrm{Ry}m^*/m_e$ for the energy and $a_B^* = a_B m_e/m^*$ for the length. Here $\mathrm{Ry} = 13.6058$ eV is 1 Ry, and $a_B = 0.0529$ nm is 1 bohr radius, and m_e is the free electron mass. In the Système International (SI) system of units $\beta = eB/2\hbar$. Notice that $(2\beta)^{-1/2}$ is the radius of the ground state cyclotron orbit. After replacing $\mathbf{k}_x$ with $-i\partial/\partial x$ and k_y with $-i\partial/\partial y$, Eq. (1) is cast in the x-y coordinates and polar coordinates (r,θ) as

$$\begin{bmatrix} H_{0\pm} - E & H_+ \\ H_- & H_{0\pm} - E \end{bmatrix} \begin{bmatrix} \Psi_1(r,\theta) \\ \Psi_2(r,\theta) \end{bmatrix} = 0, \tag{2}$$

$$H_{0\pm}(x,y) = H_0'(x,y) - 2i\beta\left(y\frac{\partial}{\partial x} - x\frac{\partial}{\partial y}\right) \pm \frac{1}{4}g\mu_B B, \tag{3}$$

$$H_{0\pm}(r,\theta) = H_0'(r,\theta) + i2\beta\frac{\partial}{\partial\theta} \pm \frac{1}{4}g\mu_B B,$$

$$H_{\pm} = \alpha\left[\left(\pm\frac{\partial}{\partial x} - i\frac{\partial}{\partial y}\right) - \beta(x \mp iy)\right]$$

$$= \alpha e^{\mp i\theta}\left(\pm\frac{\partial}{\partial r} - \frac{i}{r}\frac{\partial}{\partial\theta} - \beta r\right), \tag{4}$$

where $1/4g\mu_B B$ is the Zeeman splitting for the spins up (+) and down (−). Here, the operator H_0' describes the two-dimensional isotropic harmonic oscillator in the x-y and polar coordinate systems and is given by

$$H_0'(x,y) = -\left(\frac{\partial^2}{\partial x^2} + \frac{\partial^2}{\partial x^2}\right) + \left(\beta^2 + \frac{1}{4}e_0^2\right)(x^2 + y^2),$$

$$H_0'(r,\theta) = -\left(\frac{\partial^2}{\partial r^2} + \frac{1}{r}\frac{\partial}{\partial r} + \frac{1}{r^2}\frac{\partial^2}{\partial\theta^2}\right) + \left(\beta^2 + \frac{1}{4}e_0^2\right)r^2, \tag{5}$$

where $e_0 = \hbar\omega_0$ is the characteristic energy of the confinement potential V_c. The eigenvalue problems for Eq. (5) is $H_0'\chi = \varepsilon\chi$, where ε is the eigenvalue, and χ is the eigenfunction. Because of the additional contribution of the magnetic field to the confinement potential V_c, we set $e' = (4\beta^2 + e_0^2)^{1/2}$ as a new characteristic energy. For the oscillator in the x-y coordinates, both ε and χ are

$$\chi_{m,n}(x,y) = X_m(x)Y_n(y),$$

$$X_m(x) = (\sqrt{\pi}2^m m! x_0)^{-1/2}\exp(-q_x^2/2)H_m(q_x),$$

$$m = 0,1,2,\dots,$$

$$Y_n(y) = (\sqrt{\pi}2^n n! y_0)^{-1/2}\exp(-q_y^2/2)H_n(q_y),$$

$$n = 0,1,2,\dots, \tag{6}$$

$$\varepsilon_{m,n} = e'(m+n+1),$$

$$x_0 = y_0 = \sqrt{\frac{2}{e'}},$$

where H_n is the nth Hermite polynominal. We define $q_x = x/x_0$ and $q_y = y/y_0$ with the respective classical turning points $x_0 = y_0$. For the oscillator in the polar coordinates, both ε and χ are

$$\chi_{k,m}(r,\theta) = R_{k,m}(r)\Phi_m(\theta),$$

$$\Phi_m(\theta) = \frac{1}{\sqrt{2\pi}}e^{im\theta}, \quad m = 0, \pm 1, \pm 2, \dots,$$

$$R_{k,m}(r) = \frac{1}{r_0}\left[2\frac{k!}{(k+|m|)!}\right]^{1/2}e^{-\mu/2}\mu^{|m|/2}L_k^{|m|}(\mu),$$

$$k = 0,1,2,3,\dots, \tag{7}$$

$$r_0 = \sqrt{\frac{2}{e'}}$$

where $L_k^{|m|}$ is the associated Laguerre polynomial. Here we define $\mu = r/r_0$, where the classical turning point is r_0.

To solve the eigenvalue problem of Eq. (2), we expand Ψ_j $(j=1,2)$ into a linear combination of a set of orthonormal basis functions and adopt the two-dimensional isotropic harmonic oscillator wave functions $\chi_{k,m}(r,\theta)$ in the polar coordinates as the basis:[22,26]

$$\Psi_j(r,\theta) = \sum_{km} A_{km}^{(j)}\chi_{k,m+j-1}(r,\theta), \quad j=1,2 \tag{8}$$

where $A_{km}^{(j)}$ are the appropriate expansion coefficients to be determined. By substituting Ψ_j of Eq. (8) into Eq. (2), multiplying Eq. (2) by $R_{k'm'}\Phi_{m'}$, and integrating over the entire x-y plane, we obtain a matrix equation which becomes independent of θ. We have

$$\sum_k [(\langle m,k'|H_0|m,k\rangle - E\delta_{k',k})A_{k,m}^{(1)} + \langle m,k'|H_+|m$$

$$+ 1,k\rangle A_{k,m}^{(2)}]\delta_{m',m} = 0$$

$$\tag{9}$$

$$\sum_k [\langle m+1,k|H_-|m,k\rangle A_{k,m}^{(1)} + (\langle m+1,k'|H_0|m+1,k\rangle$$

$$- E\delta_{k',k})A_{k,m}^{(2)}]\delta_{m',m+1} = 0$$

This procedure significantly simplifies the numerical calculations. After solving the matrix equation, the eigenenergies E and the expansion coefficients $A_{km}^{(j)}$ are determined. The

polarization P of the system is calculated to be

$$P = \sum_{k,m} (|A_{k,m}^{(1)}|^2 - |A_{k,m}^{(2)}|^2),$$

$$\sum_{k,m} (|A_{k,m}^{(1)}|^2 + |A_{k,m}^{(2)}|^2) = 1, \tag{10}$$

where the double sums of the first (second) term give the total probability of the electron with spin up (down), and the coefficients $A_{km}^{(j)}$ are normalized.

Another approach to solve Eq. (2) is to expand Ψ_j into a linear combination of a set of orthonormal basis functions using the two-dimensional isotropic harmonic oscillator wave functions $\chi_{mn}(x,y)$ in the x-y coordinates as the basis:

$$\Psi_j(x,y) = \sum_{mn} B_{mn}^{(j)} \chi_{m,n}(x,y), \quad j = 1,2 \tag{11}$$

where $B_{mn}^{(j)}$ are the appropriate expansion coefficients to be determined. By substituting Ψ_j of Eq. (11) into Eq. (2) we use the same procedure as we did in the case of polar coordinates to obtain a matrix equation. The advantages of using $\Psi_j(x,y)$ are that the matrix elements can be evaluated analytically and the final matrix equation is Hermitian. The result of using $\Psi_j(r,\theta)$ in polar coordinates is that the final matrix equation is a real asymmetric matrix.

To serve as a guide line, let us consider the simplest case of $m=0,1$ and $n=0,1$ with $B=0$ in Eq. (6) in the x-y coordinates. We obtain an 8×8 Hermitian matrix from the matrix equation. Let us define the following quantities: $e_0 = \hbar \omega_0$ and $a = \frac{1}{2} \alpha e_0^{1/2}$ in the effective atomic units. The eigenvalues E_j ($j = 0-7$) have analytical forms which are calculated to be

$$E_j = (3e_0 \pm p)/2, \quad (5e_0 \pm p)/2, \quad (3e_0 \pm q)/2,$$

$$(5e_0 \pm q)/2, \tag{12}$$

with $p = (e_0^2 + 8a^2)^{1/2}$, $q = p$ (doubly degenerate).

As an application, the magnetization M at a finite temperatures T is calculated from the free energy F_r. Let the number of electrons in the quantum disk be N_e, which is governed by the Fermi-Dirac distribution:

$$N_e = \sum_{n=1} \frac{1}{1 + \exp[(E_n - E_F)/k_B T]},$$

$$F_r = E_F N_e - k_B T \sum_{n=1} \ln\left[1 + \exp\left(\frac{E_F - E_n}{k_B T}\right)\right], \tag{13}$$

$$M = \frac{\partial F_r}{\partial B},$$

where E_f is the Fermi energy, k_B is the Boltzmann constant and E_n's are all possible electron eigenenergies of the system.

To end this section, we have a comment on Ref. 21 Let the angular momentum in the z direction be L_z. Although the commutator $[L_z, H_0]$ is zero, the commutator $[L_z, H_\pm]$ is not zero because of the $e^{\pm i\theta}$ terms in Eq. (4). We conclude that the azimuthal quantum number m is not a good quantum number when the Rashba spin-orbit interaction is taken into
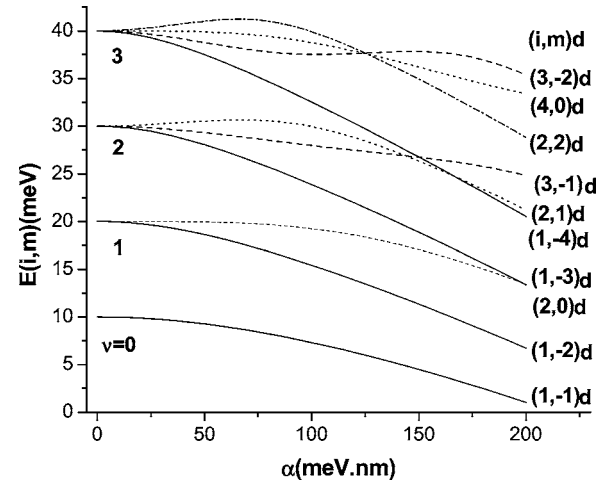

FIG. 1. Eigenenergy $E(i,m)$ vs α with $B=0$ and $e_0=10$ meV.

account. Therefore, we need to use a wave function in which a summation over m as shown in Eq. (8) is necessary. Reference 21 oversimplified their calculations by assuming that m is a good quantum number, and a linear combination over m in their wave function expansion was not used. In this work, we expect to see entirely different numerical results from those reported in Ref. 21 because the z component of the angular momentum no longer represents a good quantum number in the presence of the Rashba spin-orbit interaction. Moreover, in the model used in Ref. 24, states with only adjacent angular momentum quantum number were coupled together by the SOI, while here we have shown that the SOI mixes states of all different angular momentum quantum numbers.

III. NUMERICAL RESULT AND DISCUSSION

For our numerical calculations, we choose Eq. (7) in polar coordinates as the orthogonal set of basis functions and setting $0 \leq k \leq 20$ we obtain a matrix equation with a dimension $N=42$ from Eq. (2). The oscillator wave fuctions in the x-y coordinate system in Eq. (6) with $0 \leq m \leq 20$ and $0 \leq n \leq 20$ yield a Hermitian matrix, with a dimension of $N=441$, and is employed to check our numerical results. For InAs, the effective electron mass $m^*=0.023m_e$ and the Landé factor for the electron[16] $g=-8$ are used in our calculations. We calculate the lowest five eigenvalues for each azimuthal quantum number m: $E(i,m)$, $i=1-5$. By examining the convergence of the eigenvalues, the matrix equation with $N=42$ guarantees that the errors in the largest eigenvalue E_5 are less than 10^{-5} meV.

We realize that for the two-dimensional isotropic harmonic oscillator the νth excited state has a degeneracy of $\nu+1$, where $\nu=1,2,3,\ldots$ and the ground state is $\nu=0$. In the absence of the magnetic field ($B=0$), the variation of the eigenenergy $E(i,m)$, with the Rashba SOI parameter α, for $e_0=10$ meV is shown in Fig. 1. When α is zero, the two coupled equations for spins up and down shown in Eq. (2) are decoupled because of $H_\pm=0$ and $H_{0\pm}$ reduce to H_0' (the Hamiltonian for the isotropic simple harmonic oscillator) because $B=0$. Figure 1 shows that at $\alpha=0$ the νth excited state has $\nu+1$ doubly degenerate levels due to the
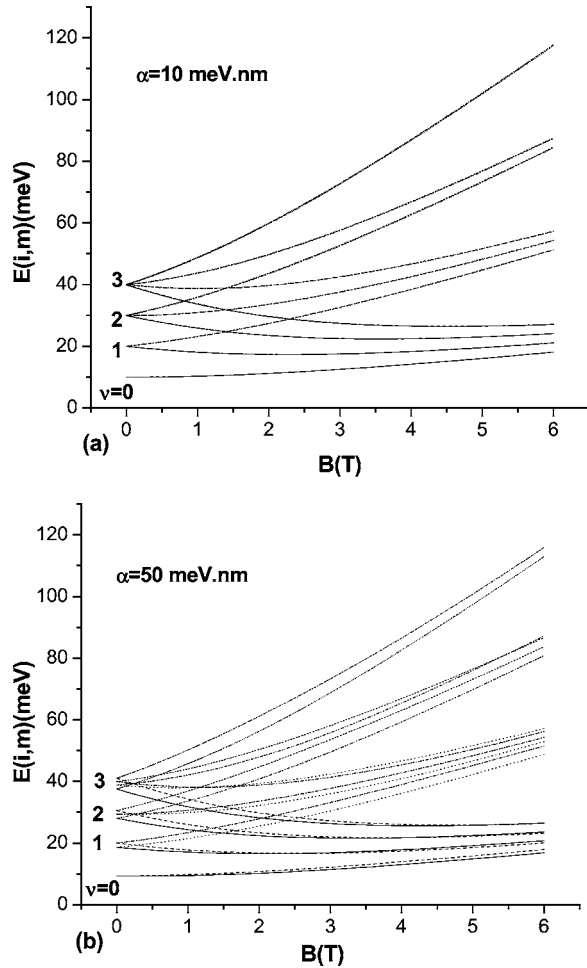
FIG. 2. Eigenenergy $E(i,m)$ vs B for $e_0 = 10$ meV with (a) $\alpha = 10$ meV nm and (b) $\alpha = 50$ meV nm.

FIG. 3. Probability densities $\rho_j(j=1,2)$ as a function of x with $B=1$ T, $\alpha=50$ meV nm, and $e_0=10$ meV for (a) the $(2,-1)$ state and (b) the $(4,0)$ state. Solid curves for $j=1$ (spin up marked with u) and dotted curves for $j=2$ (spin down marked with d).

spins and each level has an oscillator energy of $(\nu+1)e_0$. Each level of $E(i,m)$ is labeled as $(i,m)d$ or $(i,m)u$, where u and d are used to indicate the spin states up (u) and down (d). The spin up or down state is determined by examining the wave functions Ψ_1 and Ψ_2 in Eq. (2). A discussion of the probability densities ($=\Psi_j^*\Psi_j$, $j=1,2$) for the spins is presented later. The lowest 20 levels of $E(i,m)$ are labeled as follows: for $\nu=0[(1,-1)d,(1,0)u]$; for $\nu=1[(1,1)u,(2,0)d,(1,-2)d,(2,-1)u]$; for $\nu=2[(1,2)u,(2,1)d,(3,-1)d,(3,0)u,(1,-3)d,(2,-2)u]$; for $\nu=3[(1,3)u,(2,2)d,(3,1)u,(4,0)d,(3,-2)d,(4,-1)u,(1,-4)d,(2,-3)u]$. For $\alpha>0$ all the energy levels are doubly degenerate for spins up and down; thus only the $E(i,m)$'s with spin down $(i,m)d$ are plotted in Fig. 1. The lowest energy level obtained from Eq. (9) is $E(1,-1)=9.969\,86$ meV, while $E(1,-1)$ approximated by Eq. (12) is 9.97 meV for $\alpha=10$ meV nm. So long as $B=0$ and $\alpha<15$ meV nm, Eq. (12) gives a good estimate for $E(1,-1)$. With $\alpha=10$ meV nm and $e_0=10$ meV, $E(i,m)$ vs B is plotted in Fig. 2(a) for the lowest 20 levels. When $B=0$, there are $\nu+1$ doubly degenerate levels. When $B>0$, all the degeneracies are lifted to yield $2(\nu+1)$ levels for $\nu=0,1,2,3$ but the energy splittings are too small to be shown in Fig. 2(a). If we choose $\alpha=50$ meV nm and $e_0=10$ meV, the $E(i,m)$ vs B curves plotted in Fig. 2(b) show clearly that there are 20 different levels due to the
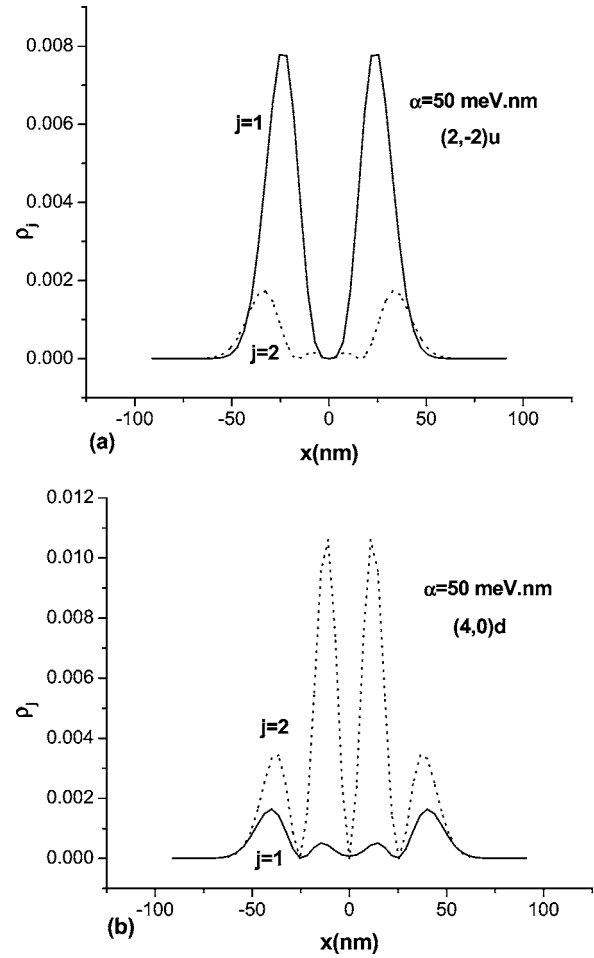
energy splitting. The probability densities are $\rho_j=|\Psi_j|^2$, where $j=1$ is for spin up and $j=2$ is for spin down [see Eq. (2)] with $\rho_1+\rho_2=1$. The probability densities as a function of $x=r\cos\theta$ with $B=1$ T, $e_0=10$ meV and $\alpha=50$ meV nm for the eigenenergies $E(2,-2)$ and $E(4,0)$ are plotted in Figs. 3(a) and 3(b), respectively. In order to show both ρ_1 and ρ_2, α is intentionally chosen to be large. Figure 3(a) shows that ρ_1 is the dominant component, and thus the $(2,-2)$ state is labeled with u (spin up) with a polarization of $P=+0.54$, while Fig. 3(b) shows that ρ_2 is the dominant component, and thus the $(4,0)$ state is labeled with d (spin down) with a polarization of $P=-0.49$.

The energy splittings ΔE_j as a function of B for $\alpha=10$ meV nm and $e_0=10$ meV are plotted in Fig. 4 with $E(1,0)-E(1,-1)$ labeled as ΔE_1, $E(2,0)-E(1,1)$ labeled as ΔE_2, and $E(2,-1)-E(1,-2)$ labeled as ΔE_3. Solid curves are evaluated with $g=-8$ (including Zeeman splitting), while dashed curves are evaluated with $g=0$ (excluding Zeeman splitting).

The energy splittings for the lowest two energy levels $\Delta E_1=E(1,0)-E(1,-1)$ vs B for $\alpha=10, 30, 50$ mev nm with $e_0=10$ meV are plotted in Fig. 4(a). Here we observe that ΔE_1 can be suppressed due to the Zeeman splitting with $g=-8$. Notice that ΔE_1 is small; even when B is 6 T, ΔE_1 is
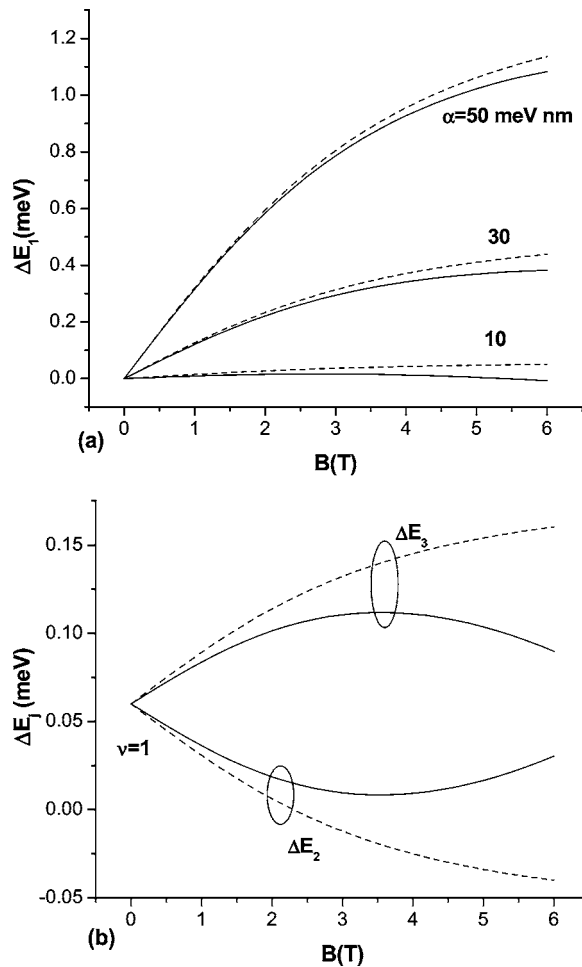
FIG. 4. Energy splitting ΔE_j as a function of B with $e_0 = 10$ meV for (a) ΔE_1, $\alpha = 10$, 30, and 50 meV nm, and for (b) ΔE_2, ΔE_3 with $\alpha = 10$ meV nm. Solid (dotted) curves represent Zeeman splitting included (excluded). [$\Delta E_1 = E(1,0) - E(1,-1)$, $\Delta E_2 = E(2,0) - E(1,1)$, and $\Delta E_3 = E(2,-1) - E(1,-2)$]

FIG. 5. Polarization P as a function of B with $e_0 = 10$ meV and $\alpha = 10$, 20, 30, 40, and 50 meV nm for (a) $(1,-1)$ and (b) $(2,-1)$ states.

only 0.05 meV. However, ΔE_1 can increase rapidly as α increases. Figure 4(b) shows that the energy splittings for the excited states ΔE_2 and ΔE_3 vs B. Both ΔE_2 and ΔE_3 calculated with the Zeeman splitting differ significantly from ΔE_2 and ΔE_3 calculated without the Zeeman splitting. The polarization P defined in Eq. (10) versus B for $\alpha = 10, 30, 50$ meV nm with $e_0 = 10$ meV is plotted in Fig. 5(a) for the lowest state $(1,-1)$ and Fig. 5(b) for the excited state $(2,-1)$. Figure 5(a) shows that when α is small the variation of P with B is negligible (≈ -0.99 spin down), but when α is larger the variation of P with B becomes stronger. This rapid change in P with B is even more evident for the $(2,-1)$ state as shown in Fig. 5(b). It is interesting to note that in Fig. 5(b) when B is larger than 4.8 T, the polarization P changes sign from positive to negative.

As an application of our numerical calculations for $E(i, m)$, we discuss how the Fermi energy E_f and the magnetization M of the quantum disk at 0° K vary with B for the case of $e_0 = 10$ meV with strong SOI $\alpha = 50$ meV nm for various N_e's. Let us assume that the total number of electrons in the system is a constant, then N_e in Eq. (13) indicates that E_f must vary with B in order to keep N_e constant. We use 30 $E(i, m)$ levels to plot Fig. 6. Figure 6(a) shows that
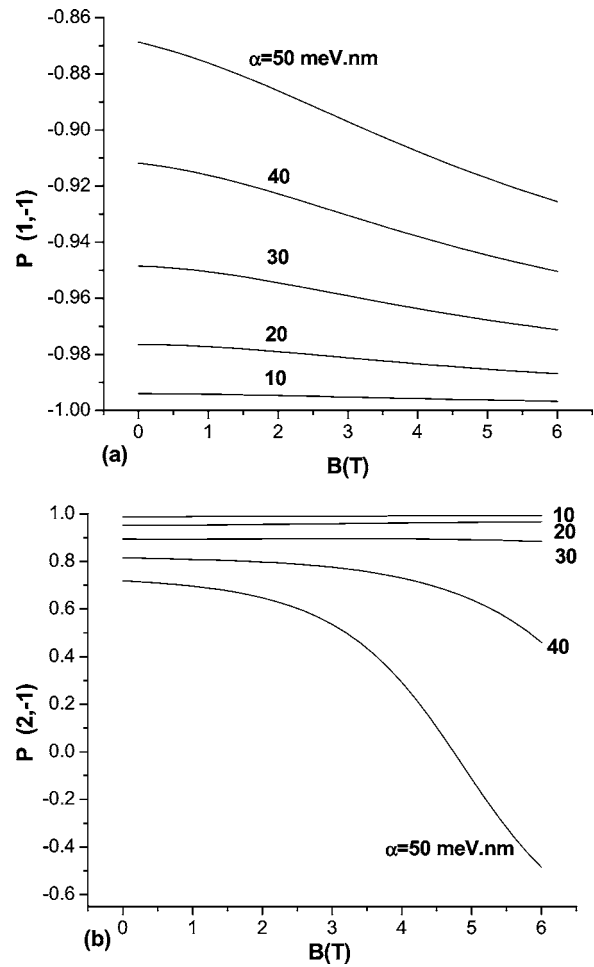
(1) when N_e is 2, E_f increases monotonically as B increases; (2) when N_e is 4, E_f shows a small peak located at $B \approx 0.3$ T because crossing occurs between the $[(2,0)d$ and $(1,2)d]$ states as depicted in Fig. 2(b); (3) when N_e is 6, E_f shows two small peaks located at $B \approx 1.2$ T and 1.65 T because crossings occur between the $[(2,-1)d$ and $(1,2)d]$ states and between the $[(2,-1)u, (2,1)d]$ states, respectively, as depicted in Fig. 2(b); (4) when N_e is 8, E_f shows three small peaks located at $B \approx 0.3$, 2.1, and 2.55 T. At 0 K, M in Eq. (13) reduces to $\partial E_{\text{tot}} / \partial B$, where E_{tot} is the total electron energy of the system. M as a function of B is plotted in Fig. 6(b) and shows oscillatory behavior. The more electrons in the disk, the more oscillations occur in M as a function of B.

IV. CONCLUSION

We have calculated the electron energy levels for quantum disks with parabolic potential profiles in a magnetic field by solving a 2×2 single electron Hamiltonian for electron spins including the Rashba SOI. We showed that in the presence of the spin-orbit interaction, the azimuthal quantum number m is no longer a good quantum number, and found that the doubly degenerate electron energy levels $E(i, m)$ decrease as α increases and crossing occurs between energy levels. When the magnetic field B is turned on, the double degeneracy in the energy levels is removed, and the νth
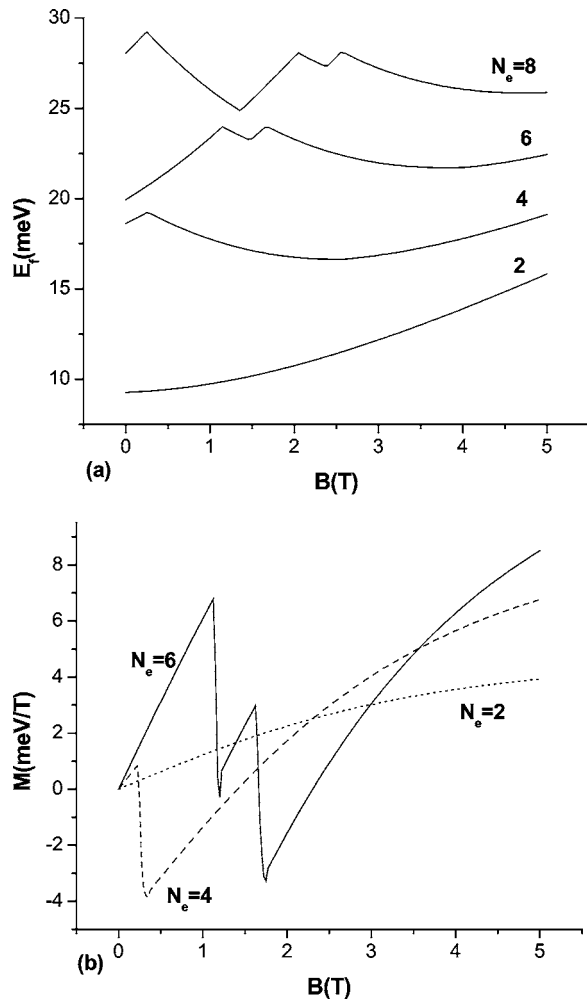
FIG. 6. (a) The Fermi energy E_F and (b) magnetization M vs B for α =50 meV nm with e_0=10 meV.

excited state splits into $2(\nu+1)$ levels. The spin states are determined by examining the wave functions for each corresponding eigenvalue $E(i,m)$. The energy splitting ΔE_j and the polarization $|P|$ increase as α and B increase. The Landé factor of the electron spin for InAs ($g=-8$) can affect the value of $\Delta E_j(B)$ significantly. The Fermi level versus B shows oscillations because of the crossing behavior between states $E(i,m)$'s. The magnetization versus B also shows oscillatory behavior.

[1] A. Kuzmich and E. S. Polzik, Appl. Phys. Lett. **85**, 5639 (2000).
[2] A. Barenco, D. Deutch, and A. Ekert, Phys. Rev. Lett. **73**, 4083 (1995).
[3] D. P. DiVincenzo, Phys. Rev. A **51**, 1015 (1995).
[4] J.-P. Leburton, S. Nagaraja, P. Matagne, and R. M. Martin, Microelectron. J. **34**, 485 (2003).
[5] J. H. Smet, R. A. Deutschmann, F. Ertl, W. Wegscheider, G. Abstreiter, and K. von Klitzing, Nature (London) **415**, 281 (2002).
[6] E. I. Rashba, Fiz. Tverd. Tela (Leningrad) **2**, 1224 (1960); [Sov. Phys. Solid State **2**, 1109 (1960)]; Y. A. Bychkov and E. I. Rashba, J. Phys. C **17**, 6039 (1984).
[7] J. C. Egues, G. Burkard, and D. Loss, Phys. Rev. Lett. **89**, 176401 (2002).
[8] E. I. Rashba and Al. L. Efros, Phys. Rev. Lett. **91**, 126405 (2003).
[9] J. Nitta, T. Akazaki, H. Takayanagin, and T. Enoki, Phys. Rev. Lett. **78**, 1335 (1997).
[10] D. Grundler, Phys. Rev. Lett. **84**, 6074 (1999).
[11] F. E. Meijer, A. F. Morpurgo, T. M. Klapwijk, T. Koga, and J. Nitta, Phys. Rev. B **70**, 201307 (2004).
[12] S. Datta and B. Das, Appl. Phys. Lett. **56**, 885 (1990).
[13] S. A. Tarasenko and N. S. Averkiev, JETP Lett. **75**, 552 (2002).
[14] X. F. Wang and P. Vasilopoulos, Phys. Rev. B **67**, 085313 (2003).
[15] G. Usaj and C. A. Balseiro, Phys. Rev. B **70**, 041301R (2004).
[16] S. Debald and B. Kramer, Phys. Rev. B **71**, 115322 (2005).
[17] T. Chakraborty and P. Pietiläinen, Phys. Rev. B **71**, 113305R (2005).
[18] P. Lucignano, B. Jouault, A. Tagliacozzo, and B. L. Altshuler, Phys. Rev. B **71**, 121310R (2005).
[19] M. G. Pala, M. Governale, U. Zülicke, and G. Iannaccone, Phys. Rev. B **71**, 115306 (2005).
[20] S. Bandyopadhyay and M. Cahay, Superlattices Microstruct. **32**, 171 (2002).
[21] W. H. Kuan, C. S. Tang, and W. Xu, J. Appl. Phys. **95**, 6368 (2004).
[22] T. Chakraborty and P. Pietiläinen, Phys. Rev. B **71**, 113305 (2005).
[23] S. Debald and C. Emary, Phys. Rev. Lett. **94**, 226803 (2005).
[24] E. T. Jaynes and F. W. Cummings, Proc. IEEE **51**, 89 (1963).
[25] F. M. Hashimzade, A. M. Babayev, S. Cakmak, and S. Cakmaktepe, Physica E (Amsterdam) **25**, 78 (2004).
[26] E. N. Bulgakov and A. F. Sadreev, JETP Lett. **73**, 505 (2001).
[27] S. Raymond *et al.*, Phys. Rev. Lett. **92**, 187402 (2004).